Blind Calibration of a Bandpass Sampling Nonuniformly Interleaved Two-Channel ADC

Bernard C. Levy, *Fellow, IEEE,* Anthony Van Selow and Mansoor S. Wahab, *Student Member, IEEE,*

***Abstract*—A method was proposed in [1] to sample directly the complex envelope of a bandpass signal by using two nonuniformly interleaved analog-to-digital converters (ADCs). The computation of the envelope samples requires two digital FIR filters and a discrete-time demodulator. To mitigate the effect of gain timing mismatches, we describe a blind calibration technique which assumes that there exists a frequency band where the envelope signal has no power, due for example to oversampling. Mismatches give rise to errors in this band, which are extracted and used to estimate adaptively the gain and timing skew mismatches. Computer simulations for an envelope consisting of a sum of complex exponentials and for a bandlimited white noise envelope demonstrate the effectiveness of the proposed calibration method.**

***Keywords*—adaptive filtering, bandpass sampling, blind calibration, direct sampling, software defined radio, stochastic gradient, time interleaved A/D converter**

I. Introduction

Due to their lower hardware complexity, direct bandpass sampling front ends have become attractive for software defined radio and radar, and for global navigation satellite system (GNSS) receivers. However, the implementation of flexible high-resolution bandpass sampling systems presents some challenges. If a single ADC is used, and B represents the occupied bandwidth of the signal of interest (which differs from its maximum frequency), alias-free reconstruction of the bandpass signal is not guaranteed for all sampling frequencies Ω_s above the Nyquist frequency $2B$ [2], [3], [4, Sec. 6.4]. In addition to being greater than $2B$, Ω_s needs to satisfy conditions which ensure that aliasing does not take place between the negative and positive frequencies of the bandpass signal to be sampled. It was shown in [2], that this difficulty can be overcome by using second-order sampling, i.e. time-interleaved sampling, where two separate ADCs operating with a time skew sample the signal with frequency $\Omega'_s = \Omega_s/2$. In this case, except for certain forbidden values of the timing offset between the two ADCs, the bandpass signal can be reconstructed from the two time-interleaved sample sequences for all sampling frequencies Ω_s above $2B$.

Whereas [2] and subsequent works [5], [6] focus on the reconstruction of the bandpass signal signal itself from its samples, for modulated signal, it is often of greater interest to obtain the sampled I and Q signal components, i.e., the sampled complex envelope of the signal. A method is described in [1] to compute the sampled complex envelope of a bandpass signal directly from the sequences produced by a two-channel time-interleaved ADC (TIADC) with timing offset dT'_s, where $0 < d < 1$ and $T'_s = 2\pi/\Omega'_s$ denotes the sub-ADC sampling period. No assumption is made about the carrier frequency Ω_c, signal bandwidth B, sampling frequency Ω_s and timing offset d, except that the sampling frequency Ω_s should be above $2B$ and the carrier frequency $\Omega_c > B/2$, which ensures that the signal considered is a bandpass signal. However, certain timing offests are forbidden, including the offset $d = 1/2$ corresponding to uniform interleaving, since this case the interleaved ADC is functionally equivalent to a single ADC, to which the limitations noted in [3] are applicable.

The computational technique described in [1] for evaluating the complex envelope samples from the sub-ADC samples relies on two real digital FIR filter and a digital demodulator. The filters need to be recomputed if the frequency band of interest changes, but since the filters are obtained by windowing known closed form impulse responses, the recomputation is rather simple, making the proposed technique well suited for software defined radio or radar receivers. However, the performance complex envelope computation algorithm is affected by timing offset mismatches, i.e. differences between the actual offset and the one used to compute the FIR filters. The source of this sensitivity is that the model of a bandpass sampling nonuniformly interleaved ADC involves a $2\pi\ell d$ phase shift, where if k denotes the Nyquist zone of the carrier frequency Ω_c, $\ell = \lfloor k/2 \rfloor$. Hence when ℓ is large, small timing offset mismatches give rise to large phase errors which significantly affect the proposed envelope computation technique.

Another reason for examining the effect of timing mismatches is that since the uniform timing skew $d = 1/2$ is among the forbidden timing offset values, the sub-ADCs cannot share the same sample and hold (S/H). The use of different S/Hs in the two sampling paths makes it difficult to achieve exactly the desired timing offset d. It is therefore important to develop a timing and gain offset calibration scheme adapted to the bandpass sampling nonuniformly interleaved ADC architecture considered. Calibration techniques can de divided in two categories, depending on whether the normal ADC operation is is suspended during calibration phases. Foreground calibration techniques interrupt the ADC operation by using a known test signal and identify mismatches by using equalizer type of techniques [7], [8]. Background or blind methods identify mismatches while the ADC is operating normally. They rely on some a priori signal knowledge, such as the absence of signal energy in certain frequency bands

This work was supported by NSF Grant ECCS-1444086.

Bernard C. Levy and and Anthony Van Selow are with the Department of Electrical and Computer Engineering, 1 Shields Avenue, University of California, Davis, CA 95616 (emails: bclevy, apvanselow@ucdavis.edu). After receiving a BS at UC Davis, Mansoor Wahab is now a graduate student in the Department of Electrical and Computer Engineering at Cornell University, Ithaca, NY 14853 (email: sw798@cornell.edu).

(this can be achieved for example if the signal is oversampled [9], [10]) or the wide-sense stationarity of the sampled signal [11]. Foreground methods have the disadvantage of lowering the ADC throughput, whereas background methods have the advantage of being able to track continuously ADC parameter changes, but they require additional digital filtering operations.

Over the last 10 years a number of blind calibration techniques have been proposed for calibrating gain and timing mismatches [9], [11]–[14] or bandwidth mismatches [10], [15]–[17] in baseband sampling uniformly interleaved ADCs. In contrast, little attention has focused on bandpass sampling ADCs, except for [18]–[20] which propose a semi-blind scheme where an analog test signal is injected in the signal prior to digitization, and then removed from the TIADC output. This approach requires oversampling and making sure that the aliased images of the injected signal do not overlap the spectrum of the signal to be sampled. More recently, a blind method described in [21] extends the pseudo-aliasing calibration approach proposed in [14] to the bandpass case. However, all the results obtained in the bandpass case thus far concern uniformly interleaved ADCs where the goal is to sample the bandpass signal itself instead of its envelope. We propose here a different blind calibration method tailored to the envelope sampling technique of [1] which leverages the digital filtering operations used to compute the envelope in order to perform the TIADC calibration. As in [9], [10] it is assumed that the signal is slightly oversampled, by say 20%. This creates a frequency band where the complex envelope does not have any spectral content. Therefore the presence of energy in this band in the reconstructed envelope indicates that the TIADC gain and timing skew estimates used in the reconstruction are incorrect. By implementing a complex bandpass filter which extracts the signal power in this band, we construct an error signal whose power is minimized adaptively to estimate the gain and timing offset mismatches.

The paper is organized as follows. The complex envelope sampling scheme of [1] is reviewed in Section II. The blind calibration approach we propose is described in Section III. Simulation results are presented in section IV for an envelope formed by the sum of complex tones and for a bandlimited white noise envelope. It is shown that calibration leads to a significant improvement in both the SNDR and MSE of the complex envelope sampling method. Finally, conclusions are presented in Section V.

II. Complex envelope sampling

Consider a bandpass signal

$$\begin{aligned} x_c(t) &= a_c(t)\cos(\Omega_c t) - b_c(t)\sin(\Omega_c t) \\ &= \Re[c_c(t)e^{j\Omega_c t}] = |c_c(t)|\cos(\Omega_c t + \angle c_c(t)) \,, \end{aligned} \quad (1)$$

where

$$c_c(t) = a_c(t) + jb_c(t) \quad (2)$$

denotes the complex envelope of $x_c(t)$ and the in-phase and quadrature components $a_c(t)$ and $b_c(t)$ are baseband signals with bandwidth $B/2$. If the carrier frequency $\Omega_c > B/2$ (it is in general much larger), the Fourier spectrum $X_c(j\Omega)$ of $x_c(t)$ is contained in two disjoint positive and negative frequency bands $[\Omega_L, \Omega_H]$ and $[-\Omega_H, -\Omega_L]$ with $\Omega_L = \Omega_c - B/2$ and $\Omega_H = \Omega_c + B/2$, so that the occupied bandwidth of $x_c(t)$ is $\Omega_H - \Omega_L = B$. To sample the complex envelope, we consider the two-channel time-interleaved ADCs shown in Fig. 1.

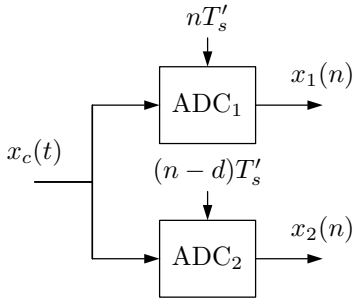

Fig. 1. Time-interleaved sampling of bandpass signal $x_c(t)$.

T'_s denotes the sampling period of the sub-ADCs, which have therefore sampling frequency $\Omega'_s = 2\pi/T'_s = \Omega_s/2$, where Ω_s denotes the sampling frequency of the overall ADC. It is assumed that $\Omega_s > 2B$, or equivalently $\Omega'_s > B$. The timing offset between the two ADCs is $D = dT'_s$ with $0 < d < 1$. For $d = 1/2$, the combination of the two sub-ADCs forms a uniform ADC with sampling period $T_s = T'_s/2$, but for $d \neq 1/2$, the overall ADC has a nonuniform but periodic sampling pattern. Although the two sub-ADCs are assumed to be matched, due to manufacturing imperfections, the second sub-ADC has a relative gain g compared to the first.

Let

$$\ell = \mathrm{round}\big(\frac{\Omega_c}{\Omega'_s}\big) \,. \quad (3)$$

so that Ω_c belongs to the frequency band $[(\ell - 1/2)\Omega'_s, (\ell + 1/2)\Omega'_s]$. Since this frequency band corresponds to the location of the ℓ-th image copy of a sampled baseband signal, it is referred to here as the ℓ-th image band. In the following it is assumed that $\ell \geq 1$, so that the signal $x_c(t)$ is a bandpass signal. Since the band $[(\ell - 1/2)\Omega'_s, (\ell + 1/2)\Omega'_s]$ corresponds to the 2ℓ-th and $2\ell + 1$-th Nyquist zones of the sub-ADCs, ℓ can be expressed in terms the index k of the Nyquist zone where Ω_c is located as $\ell = \lfloor k/2 \rfloor$. If we consider the discrete modulation frequency

$$\omega_b = \Omega_c T'_s \bmod 2\pi = \Big(\frac{\Omega_c}{\Omega'_s} - \ell\Big)2\pi \,, \quad (4)$$

so that $-\pi < \omega_b \leq \pi$, and if $c(n) = c_c(nT'_s)$ denotes the sampled complex envelope, it is shown in [1] that the sampled sequences $x_1(n)$ and $x_2(n)$ produced by the two sub-ADCs are related to $c(n)$ by the model shown in Fig. 2. In this model, the frequency response

$$F(e^{j\omega}) = ge^{-j\omega d} \quad (5)$$

with $-\pi < \omega \leq \pi$ represents the relative gain and timing skew between the two-sub-ADCs, and $G(e^{j\omega})$ is a piecewise

constant phase shift. For $\omega_b > 0$, it can be expressed as

$$G(e^{j\omega}) = \begin{cases} e^{-j2\pi(\ell+1)d} & -\pi \le \omega < -\pi + \omega_b \\ e^{-j2\pi\ell d} & -\pi + \omega_b \le \omega < \pi \,, \end{cases}$$

and for $\omega_b < 0$, we have

$$G(e^{j\omega}) = \begin{cases} e^{-j2\pi\ell d} & -\pi \le \omega \le \pi + \omega_b \\ e^{-j2\pi(\ell-1)d} & \pi + \omega_b < \omega < \pi \,. \end{cases}$$

The $\Re\{.\}$ operation in Fig. 2 takes the real part of a complex signal. Thus, from a software defined radio perspective, $G(e^{j\omega})$ depends on the carrier frequency Ω_c of the signal of interest, since it depends on its image zone index ℓ, and on its relative location ω_b within this band, but $F(e^{j\omega})$ remains the same since it depends only on the sub-ADCs relative characteristics.

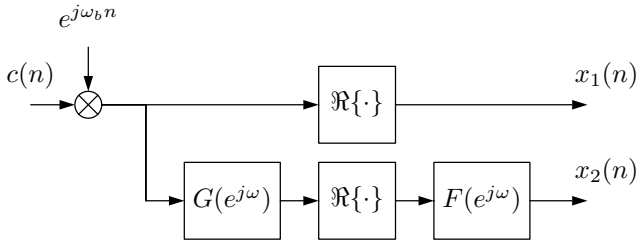

Fig. 2. Discrete-time bandpass sampling model

Let

$$\boldsymbol{\theta} = \begin{bmatrix} g \\ d \end{bmatrix}$$

denote the vector formed by the sub-ADC parameters. It was shown in [1] that the complex envelope $c(n)$ can be evaluated by passing the sub-ADC sequences $x_1(n)$ and $x_2(n)$ through digital digital filters $H_1(e^{j\omega}, d)$ and $H_2(e^{j\omega}, \boldsymbol{\theta})$ whose outputs are summed and then digitally demodulated with $e^{-j\omega_b n}$ as shown in Fig. 3. The filter $H_1(e^{j\omega}, d)$ depends on d only and is given by

$$H_1(e^{j\omega}, d) = 1 - j\cot(2\pi\ell d) \tag{6}$$

for $|\omega| \le \pi - |\omega_b|$ and

$$H_1(e^{j\omega}, d) = 1 - j\cot(\pi(2\ell + \mathrm{sgn}(\omega_b))d) \tag{7}$$

for $\pi - |\omega_b| < |\omega| \le \pi$. Similarly $H_2(e^{j\omega}, \theta)$ depends on both g and d and takes the form

$$H_2(e^{j\omega}, \boldsymbol{\theta}) = j\frac{e^{j\omega d}}{g\sin(2\pi\ell d)} \tag{8}$$

for $|\omega| \le \pi - |\omega_b|$ and

$$H_2(e^{j\omega}, \boldsymbol{\theta}) = j\frac{e^{j(\omega - \pi\mathrm{sgn}(\omega))d}}{g\sin(\pi(2\ell + \mathrm{sgn}(\omega_b)))} \tag{9}$$

for $\pi - |\omega_b| < |\omega| \le \pi$. The IIR impulse responses of filters $H_1(e^{j\omega}, d)$ and $H_2(e^{j\omega}, \boldsymbol{\theta})$ are computed in [1] and are given respectively by

$$\begin{aligned} \Re\{h_1(n,d)\} &= \delta(n) \\ \Im\{h_1(n,d)\} &= -\cot(\pi(2\ell + \mathrm{sgn}(\omega_b))d)\delta(n) \\ &\quad (\cot(\pi(2\ell + \mathrm{sgn}(\omega_b))d) - \cot(2\pi\ell d)) \\ &\quad \times \frac{\sin((\pi - |\omega_b|)n)}{\pi n} \,, \end{aligned} \tag{10}$$

and

$$\Re\{h_2(n, \boldsymbol{\theta})\} = 0$$

$$\begin{aligned} \Im\{h_2(n, \boldsymbol{\theta})\} &= \frac{\sin((\pi - |\omega_b|)(n+d))}{g\pi\sin(2\pi\ell d)(n+d)} \\ &\quad - \frac{\sin((\pi - |\omega_b|)(n+d) - \pi d)}{g\pi\sin(\pi(2\ell + \mathrm{sgn}(\omega_b))d)(n+d)} \,. \end{aligned} \tag{11}$$

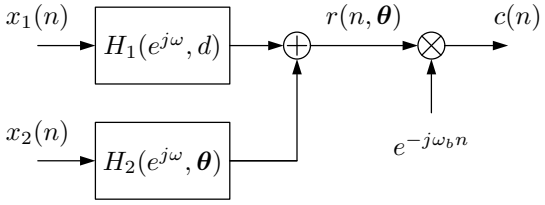

Fig. 3. Recovery of $c(n)$ from $x_1(n)$ and $x_2(n)$ by filtering and digital demodulation.

III. Blind TIADC Calibration Method

In practice, clock jitter and semiconductor process imperfections make it impossible to match exactly the two sub-ADCs to their design specifications. For a desired sub-ADC timing skew of d_0, due to circuit imperfections, the actual timing skew is d and the sub-ADC relative gain g differs from its from its ideal value $g_0 = 1$. Typically, the mismatches

$$\gamma \triangleq g - 1 \quad , \quad \delta \triangleq d - d_0 \tag{12}$$

are small, say about 1% or less, but they contribute to a significant loss of ADC resolution. Accordingly, it is desirable to implement calibration algorithms to estimate g and d. In the following the estimated parameter vector at a given time is denoted as

$$\hat{\boldsymbol{\theta}} = \begin{bmatrix} \hat{g} \\ \hat{d} \end{bmatrix} \,,$$

where $\hat{g}$ and $\hat{d}$ denote the gain and timing offset estimates. Since mismatches are small, it is assumed throughout the remainder of this paper that $\boldsymbol{\theta}$, $\hat{\boldsymbol{\theta}}$, and the nominal parameter vector

$$\boldsymbol{\theta}_0 = \begin{bmatrix} 1 \\ d_0 \end{bmatrix}$$

are close to each other. The calibration method we consider will match the gains of the two sub-ADCs, to ensure that g is properly compensated, instead of attempting to correct the mismatch of each channel gain with respect to its nominal value. This choice of calibration strategy is dictated by our

decision to adopt a blind calibration approach since, in the absence of an external reference signal, it is impossible to detect gain errors which are common to both channels.

Since the exact gain g and timing skew d are unknown, the estimated values $\hat{g}$ and $\hat{d}$ can be substituted for the exact parameter values in reconstruction network of Fig. 3 used to evaluate the complex envelope samples. However to avoid updating all the coefficients of filters $H_1(e^{j\omega}, \hat{d})$ and $H_2(e^{j\omega}, \hat{\boldsymbol{\theta}})$ each time the parameter vector vector $\hat{\boldsymbol{\theta}}$ is updated, we exploit the fact that the estimated mismatches

$$\hat{\gamma} = \hat{g} - 1 \quad , \quad \hat{\delta} = \hat{d} - d_0$$

are small by performing first order expansions

$$H_1(e^{j\omega}, \hat{d}) = H_{10}(e^{j\omega}) + \hat{\delta} H_{11}(e^{j\omega}) \tag{13}$$

$$H_2(e^{j\omega}, \hat{\boldsymbol{\theta}}) = (1 - \hat{\gamma})[H_{20}(e^{j\omega}) + \hat{\delta} H_{21}(e^{j\omega})] \tag{14}$$

with

$$H_{10}(e^{j\omega}) = H_1(e^{j\omega}, d_0) \quad , \quad H_{20}(e^{j\omega}) = H_2(e^{j\omega}, \boldsymbol{\theta}_0)$$
$$H_{11}(e^{j\omega}) = \frac{\partial H_1}{\partial d}(e^{j\omega}, d_0) \quad , \quad H_{21}(e^{j\omega}) = \frac{\partial H_2}{\partial d}(e^{j\omega}, \boldsymbol{\theta}_0)$$

of the frequency responses and impulse responses of H_1 and H_2 in the vicinity of the nominal parameter values. The impulse responses of gradient filters $H_{11}(e^{j\omega})$ and $H_{21}(e^{j\omega})$ are evaluated in Appendix A. The multiplicative term $1 - \hat{\gamma}$ in (14) is due to the fact that $H_2(e^{j\omega}, \hat{\boldsymbol{\theta}})$ is proportional to $\hat{g}^{-1}$, so that a local expansion in the vicinity of $g_0 = 1$ results in a $1 - \hat{\gamma}$ multiplicative factor. Although first order terms are sufficient for small to moderate values of ℓ, if more accurate approximations are needed second order terms could be retained. The resulting adaptive implementation of the reconstruction filters is shown in Fig. 4. Note that the four filters $H_{ij}(e^{j\omega})$ with $i = 1, 2$ and $j = 0, 1$ are fixed and only three taps equal to estimated mismatches $\hat{\delta}$ and $\hat{\gamma}$ need to be adapted.

Since the estimated parameter vector $\hat{\boldsymbol{\theta}}$ is used in the reconstruction network of Fig. 4, the output signal $r(n, \hat{\boldsymbol{\theta}})$ obtained after summing the outputs of filters $H_1(e^{j\omega}, \hat{d})$ and $H_2(e^{j\omega}, \hat{\boldsymbol{\theta}})$ differs from the exact signal $r(n, \boldsymbol{\theta}) = c(n)e^{j\omega_b n}$ that would be obtained for the correct parameter vector. Therefore we can use differences between $r(n, \hat{\boldsymbol{\theta}})$ and the correct signal $r(n, \boldsymbol{\theta})$ to calibrate the TIADC. The blind calibration scheme we propose estimates $\boldsymbol{\theta}$ adaptively by extracting from $r(n, \hat{\boldsymbol{\theta}})$ an error signal $e(n, \hat{\boldsymbol{\theta}})$ whose power provides a measure of how far the estimated vector $\hat{\boldsymbol{\theta}}$ is from the true vector $\boldsymbol{\theta}$. It is assumed that the complex envelope $c_c(t)$ is oversampled with oversampling ratio

$$\alpha = \frac{\Omega_s - 2B}{\Omega_s} \, . \tag{15}$$

In this case the periodic discrete-time Fourier transform (DTFT) $C(e^{j\omega})$ of the sampled envelope sequence $c(n)$ satisfies

$$C(e^{j\omega}) = 0$$

over interval $[(1-\alpha)\pi, (1+\alpha)\pi]$ and all its 2π-shifted copies. This implies that when the estimated parameter vector $\hat{\boldsymbol{\theta}}$ coincides with the correct vector $\boldsymbol{\theta}$, the signal $r(n, \boldsymbol{\theta}) = c(n)e^{j\omega_b n}$ has no frequency content in the band $I = [\omega_b + (1-\alpha)\pi, \omega_b + (1+\alpha)\pi]$ and its 2π-shifted copies. Consider therefore the discrete-time bandpass filter

$$H_{\rm BP}(e^{j\omega}) = \begin{cases} 1 & \omega \in I \mod (2\pi) \\ 0 & \text{otherwise} \, . \end{cases} \tag{16}$$

It can be viewed as an ideal lowpass filter for the band $[-\alpha\pi, \alpha\pi]$ modulated by $\omega_b + \pi$, so that its IIR impulse response is given by

$$h_{BP}(n) = (-e^{j\omega_b})^n \frac{\sin(\alpha\pi n)}{\pi n}$$

Then if $*$ denotes the convolution operation, let

$$e(n, \hat{\boldsymbol{\theta}}) = h_{BP}(n) * r(n, \hat{\boldsymbol{\theta}}) \tag{17}$$

denote the error signal obtained by extracting from $r(n, \hat{\boldsymbol{\theta}})$ its frequency content in the band I. Since $e(n, \hat{\boldsymbol{\theta}}) = 0$ whenever $\hat{\boldsymbol{\theta}} = \boldsymbol{\theta}$, the estimation scheme we propose minimizes adaptively the power

$$J(\hat{\boldsymbol{\theta}}) = \frac{1}{2} E[|e(n, \hat{\boldsymbol{\theta}})|^2] \tag{18}$$

of complex signal $e(n, \hat{\boldsymbol{\theta}})$. This approach is justified rigorously in Appendix B by showing that if the complex envelope random process $c(n)$ is wide-sense stationary (WSS), in the vicinity of $\boldsymbol{\theta}$ $J(\hat{\boldsymbol{\theta}})$ can be approximated by a positive definite quadratic function of $\hat{\gamma} - \gamma$ and $\hat{\delta} - \delta$, provided $c(n)$ satisfies certain spectral frequency content conditions. This ensures that by minimizing $J(\hat{\boldsymbol{\theta}})$ iteratively, starting with the nominal value

$$\hat{\boldsymbol{\theta}}(0) = \begin{bmatrix} 1 \\ d_0 \end{bmatrix} \, , \tag{19}$$

the iterates will converge to the correct true parameter vector $\boldsymbol{\theta}$.

If the gradient of function $J(\hat{\boldsymbol{\theta}})$ is available, which is typically not the case since the evaluation of the ensemble average in (18) requires knowledge of the statistics of the envelope process $c(n)$, $J(\hat{\boldsymbol{\theta}})$ can be minimized by using a steepest descent iteration of the form

$$\hat{\boldsymbol{\theta}}(n+1) = \hat{\boldsymbol{\theta}}(n) - \mu \nabla_{\hat{\boldsymbol{\theta}}} J(\hat{\boldsymbol{\theta}}(n)) \tag{20}$$

where $\mu > 0$ denotes the iteration step size, and

$$\nabla_{\hat{\boldsymbol{\theta}}} J(\hat{\boldsymbol{\theta}}) = \begin{bmatrix} \frac{\partial}{\partial \hat{g}} \\ \frac{\partial}{\partial \hat{d}} \end{bmatrix} J(\hat{\boldsymbol{\theta}}) \tag{21}$$

represents the gradient of $J(\hat{\boldsymbol{\theta}})$. In the absence of the gradient of $J(\hat{\boldsymbol{\theta}})$, we apply a *stochastic gradient approximation* [22]–[24], where the expectation in (18) is replaced by its instantaneous value, which yields the adaptive estimation algorithm

$$\hat{\boldsymbol{\theta}}(n+1) = \hat{\boldsymbol{\theta}}(n) - \mu \Re\{e^*(n, \hat{\boldsymbol{\theta}}(n)) \nabla_{\hat{\boldsymbol{\theta}}} e(n, \hat{\boldsymbol{\theta}}(n))\} \tag{22}$$

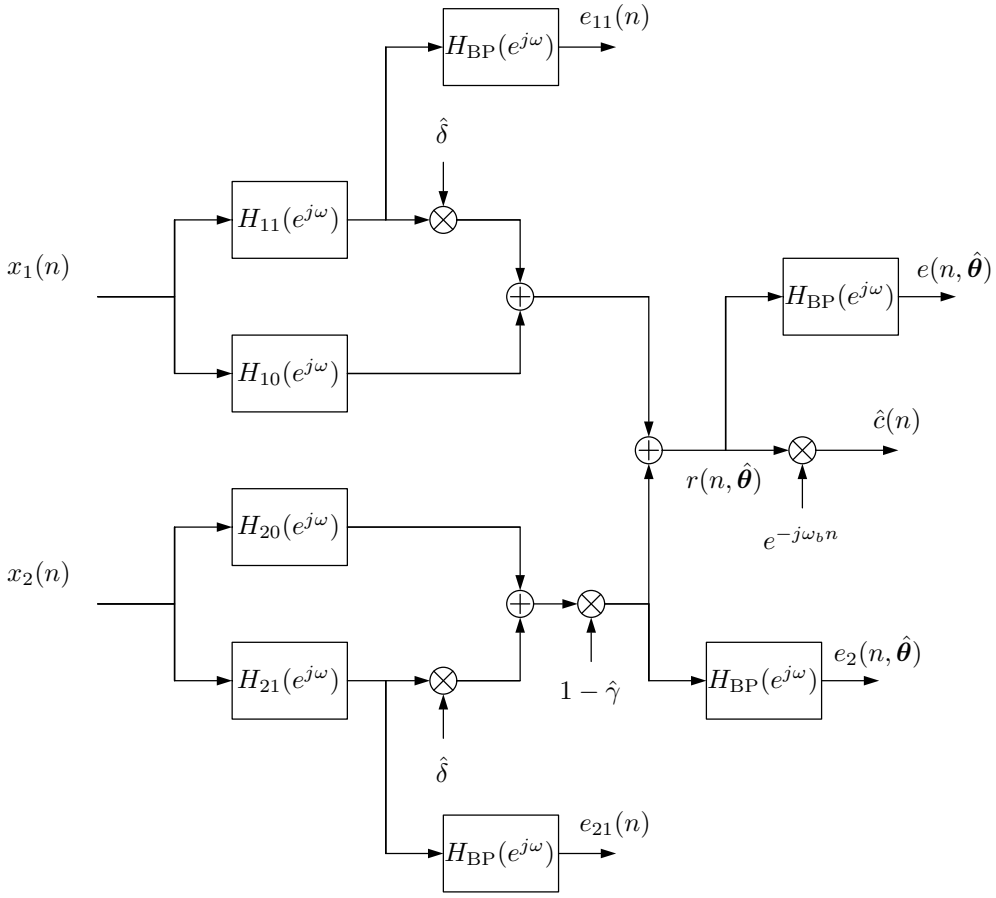

Fig. 4. Adaptive reconstruction filter implementation and error signal computation.

with initial condition (19). Typically the value of μ used for this recursion is much smaller than for the steepest descent algorithm (20), and since the recursion (22) can be interpreted as computing the average of gradient $\nabla_{\hat{\boldsymbol{\theta}}}|e^2(n,\hat{\boldsymbol{\theta}})|^2/2$, the approximation used to go from (20) to (22) just consists in replacing an ensemble average by a finite time average.

The recursion (22) requires the computation of the gradient of $e(n,\hat{\boldsymbol{\theta}})$ with respect to $\hat{\boldsymbol{\theta}}$. To perform this evaluation, it is convenient to decompose the error signal as

$$e(n,\hat{\boldsymbol{\theta}}) = e_1(n,\hat{d}) + e_2(n,\hat{\boldsymbol{\theta}}) \tag{23}$$

with

$$\begin{aligned} e_1(n,\hat{d}) &= k_1(n,\hat{d}) * x_1(n) \\ e_2(n,\hat{\boldsymbol{\theta}}) &= k_2(n,\hat{\boldsymbol{\theta}}) * x_2(n)\,, \end{aligned} \tag{24}$$

where $k_1(n,\hat{d})$ and $k_2(n,\hat{\boldsymbol{\theta}})$ denote respectively the impulse responses of filters

$$\begin{aligned} K_1(e^{j\omega},\hat{d}) &= H_{\rm BP}(e^{j\omega})H_1(e^{j\omega},\hat{d}) \\ &\approx H_{\rm BP}(e^{j\omega})[H_{10}(e^{j\omega}) + \hat{\delta}H_{11}(e^{j\omega})]\,. \end{aligned} \tag{25}$$

and

$$\begin{aligned} K_2(e^{j\omega},\hat{\boldsymbol{\theta}}) &= H_{\rm BP}(e^{j\omega})H_2(e^{j\omega},\hat{\boldsymbol{\theta}}) \\ &\approx (1-\hat{\gamma})H_{\rm BP}(e^{j\omega})[H_{20}(e^{j\omega}) + \hat{\delta}H_{21}(e^{j\omega})]\,. \end{aligned} \tag{26}$$

By using the first order expansions (25), we find that the error component signal $e_1(n,\hat{d})$ can be represented as as

$$e_1(n,\hat{d}) = e_{10}(n) + e_{11}(n)\hat{\delta}\,, \tag{27}$$

where $e_{1j}(n)$ is the signal obtained by passing $x_1(n)$ through filter $H_{\rm BP}(e^{j\omega})H_{1j}(e^{j\omega})$ with $j = 0,\,1$. Similarly, by using (26), $e_2(n,\hat{\boldsymbol{\theta}})$ can be expressed as

$$e_2(n,\hat{\boldsymbol{\theta}}) = (1-\hat{\gamma})[e_{20}(n) + e_{21}(n)\hat{\delta}]\,, \tag{28}$$

where $e_{2j}(n)$ is the signal obtained by passing $x_2(n)$ through filter $H_{\rm BP}(e^{j\omega})H_{2j}(e^{j\omega})$ for $j = 0,\,1$.

Then, by observing that only $e_2(n,\hat{\boldsymbol{\theta}})$ depends on $\hat{g}$, we find that

$$\frac{\partial e}{\partial \hat{g}}(n,\hat{\boldsymbol{\theta}}) = -\frac{1}{1-\hat{\gamma}}e_2(n,\hat{\boldsymbol{\theta}})\,. \tag{29}$$

Similarly, the derivative of $e(n,\hat{\boldsymbol{\theta}})$ with respect to $\hat{d}$ can be

expressed as

$$\frac{\partial e}{\partial \hat{d}}(n,\hat{\boldsymbol{\theta}}) = e_{11}(n) + (1-\hat{\gamma})e_{21}(n)\,. \tag{30}$$

The parameter vector estimate $\hat{\boldsymbol{\theta}}(n)$ is evaluated adaptively by substituting gradient expressions (29) and (30) inside recursion (22). Since the gradients require both the evaluation of the error $e(n,\hat{\boldsymbol{\theta}})$ and its components $e_2(n,\hat{\boldsymbol{\theta}})$, $e_{11}(n)$ and $e_{21}(n)$, and since the first-order expansions require the implementation of fixed filters H_{ij} for $i = 1,\ 2$ and $j = 0,\ 1$, eight digital filters are ultimately required to implement the proposed envelope sampling and calibration algorithm, as shown in Fig. 4. The ideal impulse responses of filters H_{ij}, $i = 1,\ 2$ $j = 0,\ 1$ and $H_{\rm BP}$ are noncausal and IIR, but causal FIR implementations of these filters can be obtained by windowing and inclusion of appropriate delays. It is also worth observing that the implementation of the four copies of bandpass filter $H_{\rm BP}$ used to generate error components e_2, e_{11} and e_{21} and error e is required only during calibration phases. After convergence, if the values of g and d are not expected to change, the estimation algorithm (20) and associated bandpass filters can be turned off to save power, until a new calibration update is required. However, if power consumption is not a significant consideration, it may be beneficial to keep running the recursion (22) in the background to track drifts in the values of g and d due to variations in TIADC operating conditions, such as temperature changes.

IV. Simulations

A. Sum of Complex Tones Complex Envelope

To illustrate the proposed TIADC calibration method, we consider first a bandpass signal with $F_c = \Omega_c/(2\pi) = 5.15$GHz, whose continuous-time envelope

$$\begin{aligned} c_c(t) &= 2\cos(400\times 10^6\times 2\pi t) \\ &\quad + j[\sin(400\times 10^6\times 2\pi t) + \cos(175\times 10^6\times 2\pi t)] \\ &= \frac{3}{2}e^{j400\times 10^6\times 2\pi t} + \frac{1}{2}e^{-j400\times 10^6\times 2\pi t} \\ &\quad + \frac{j}{2}[e^{j175\times 10^6\times 2\pi t} + e^{-j175\times 10^6\times 2\pi t}] \end{aligned} \tag{31}$$

contains 4 complex tones and has bandwidth $B/(4\pi) = 400$MHz. The sub-ADC sampling frequency $F_s' = \Omega_s'/(2\pi) = 1$GHz is above $B/(2\pi)$, and the oversampling ratio $\alpha = 0.2$. Since

$$F_c = 5F_s' + 150\,,$$

we have $\ell = 5$ and

$$\omega_b = \frac{150}{1000}\times 2\pi = 0.3\pi\,.$$

The discrete-time envelope obtained by sampling $c_c(t)$ with sampling period $T_s' = 1/F_s'$ is

$$\begin{aligned} c(n) = c_c(nT_s') &= \frac{3}{2}e^{j0.8\pi n} + \frac{1}{2}e^{-j0.8\pi n} \\ &\quad + \frac{j}{2}[e^{j0.35\pi n} + e^{-j0.35\pi n}] \end{aligned} \tag{32}$$

This signal has four tones located at $\pm 0.8\pi$ and $\pm 0.35\pi$, but the tone at 0.8π has an amplitude three times larger than the tones at -0.8π and $\pm 0.35\pi$. Note that the tone located at 0.35π is inside the frequency band

$$I_T = [0.8\pi, 1.2\pi] - 0.6\pi = [0.2\pi, 0.6\pi]$$

defined in (53), where $c(n)$ is required to have some energy to ensure that the proposed calibration method works satisfactorily. Also, the passband of filter $H_{\rm BP}(e^{j\omega})$ is $I = [0.8\pi, 1.2\pi] + 0.3\pi \mod (2\pi) = [-0.9\pi, -0.5\pi]$.

Although the nominal timing offset used in the TIADC reconstruction network of Fig. 4 is $d_0 = 0.425$, timing and gain mismatches $\delta = d - d_0 = -0.25\times 10^{-2}$ and $\gamma = g - 1 = 10^{-2}$ are present. The two sub-ADC sequences are therefore given by

$$\begin{aligned} x_1(n) &= \Re\{c(n)e^{j\omega_b n}\} + v_1(n) \\ x_2(n) &= \Re\{(f * c)(n)e^{j\omega_b(n-d)}\} + v_2(n)\,, \end{aligned} \tag{33}$$

where $f(n)$ denotes the impulse response of $F(e^{j\omega})$ and the zero mean white noises $v_1(n)$ and $v_2(n)$ model the effect of thermal and quantization noises. The sub-ADC SNR is 61.8dB.

The reconstruction filters $H_{ij}(e^{j\omega})$ with $i = 1,\ 2$ and $j = 0,\ 1$ appearing in Fig. 4 are obtained by windowing the IIR impulse responses of these filters with a Kaiser window of length 61 and parameter $\beta = 6$. The magnitude of the frequency responses of the resulting FIR filters are shown in Fig. 5. The small notches of these filters (except for H_{11}) at the frequency $\pi - |\omega_b| = 0.7\pi$ are due to phase discontinuities of the reconstruction filters (except for H_{11}) at this frequency. Note that since the magnitude of the gradient filters $H_{i1}(e^{j\omega})$ with $i = 1,\ 2$ is approximately proportional to ℓ, for the value $\ell = 5$, the gradient filters have a large magnitude, suggesting that for large values of ℓ, higher terms should be retained in expansions (13) and (14) of the reconstruction filters. To ensure that the transition region of the bandpass filter $H_{\rm BP}(e^{j\omega})$ does not extend outside $[-0.9\pi, -0.5\pi]$, we select a value $\alpha = 0.15$ (corresponding to a narrower passband of $[-0.85\pi, -0.55\pi]$) in the impulse response $h_{\rm BP}(n)$ and employ a Kaiser window of length 81 and parameter $\beta = 8$.

For the 4 tones complex envelope considered, the blind estimation algorithm (22) is applied to a sequence of length $L = 5\times 10^4$ samples. The initial mismatches are selected as $\hat{\gamma} = 0$ and $\hat{\delta} = 0$, which corresponds to the selecting the nominal TIADC parameters. Instead of using the same step size for both the gain and timing offset mismatches, we select $\mu_\gamma = 10^{-3}$ and $\mu_\delta = 10^{-5}$ for improved speed of convergence and estimation accurcay. This choice can be interpreted as replacing the steepest descent algorithm by a quasi-Newton algorithm. The resulting gain and time-delay mismatches are shown in Fig. 6 and Fig. 7 respectively. Note that the final estimated gain mismatch value $\hat{\gamma}(L) = 0.77\times 10^{-2}$ underestimates the gain mismatch by more than 20%, but the estimated timing offset mismatch $\hat{\delta}(L) = -0.27\times 10^{-2}$ is very close to the exact mismatch value δ.

To demonstrate the performance improvement of the proposed calibration algorithm, Fig. 8 and Fig. 9 show the power spectral densities (PSDs) of the reconstructed envelope $\hat{c}(n)$

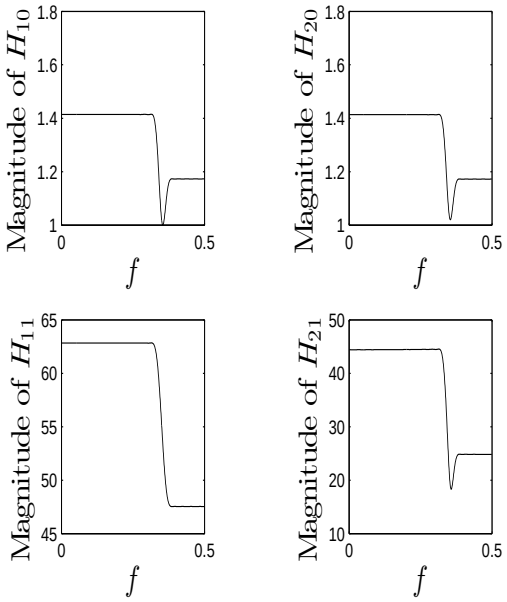

Fig. 5. Magnitudes of FIR approximation of reconstruction filters H_{ij} with $i = 1,\ 2$ and $j = 0,\ 1$ for a Kaiser window of length $M = 61$ and parameter $\beta = 6$.

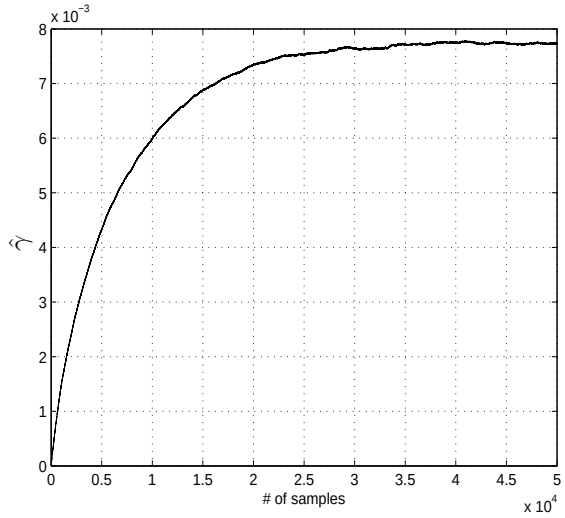

Fig. 6. Gain mismatch estimates for a 4 tone complex input sequence of length $L = 5 \times 10^4$ samples, and adaptation step sizes $\mu_\gamma = 10^{-3}$ amd $\mu_\delta = 10^{-5}$.

obtained before and after calibration. Before calibration, the sampled envelope is computed by using the reconstruction filters $H_{10}(e^{j\omega})$ and $H_{20}(e^{j\omega})$ computed for the nominal TIADC values, whereas the calibrated sequence $\hat{c}(n)$ uses the last 10^4 estimates $\hat{\gamma}(n)$ and $\hat{\delta}(n)$ produced by the blind estimation algorithm. Note that as indicated by Fig. 6 and Fig. 7, the blind estimation algorithm converges quickly, so that the

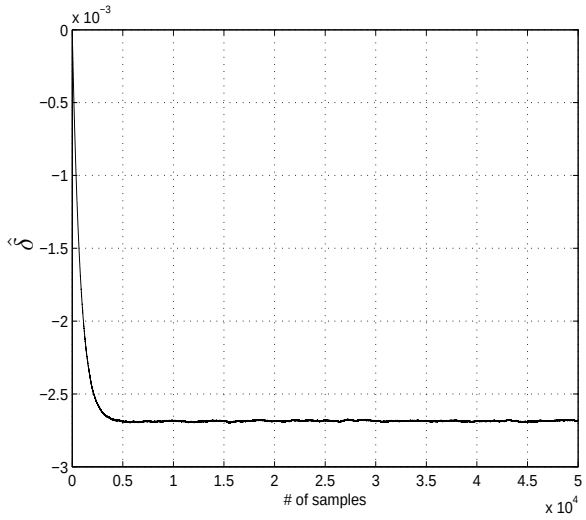

Fig. 7. Timing offset mismatch estimates for a 4 tone complex input sequence of length $L = 5 \times 10^4$ samples, and adaptation step sizes $\mu_\gamma = 10^{-3}$ amd $\mu_\delta = 10^{-5}$.

mismatch estimates obtained during the final 10^4 simulation samples fluctuate around the final values.

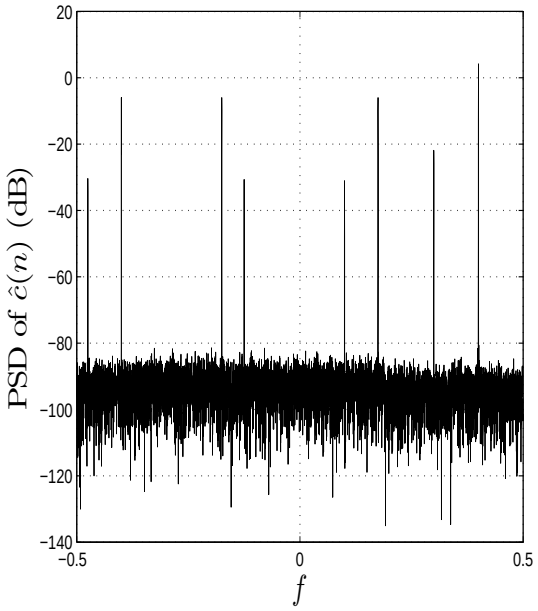

Fig. 8. PSD of the estimated envelope $\hat{c}(n)$ before calibration.

The MSE and SFDR before calibration are -17.80dB and 25dB, and -36.51dB and 43dB after calibration, respectively. Thus calibration yields about 18dB in MSE and SFDR improvement.

Next, to assess the effect of the image band index ℓ on the performance of the proposed calibration algorithm, we perform

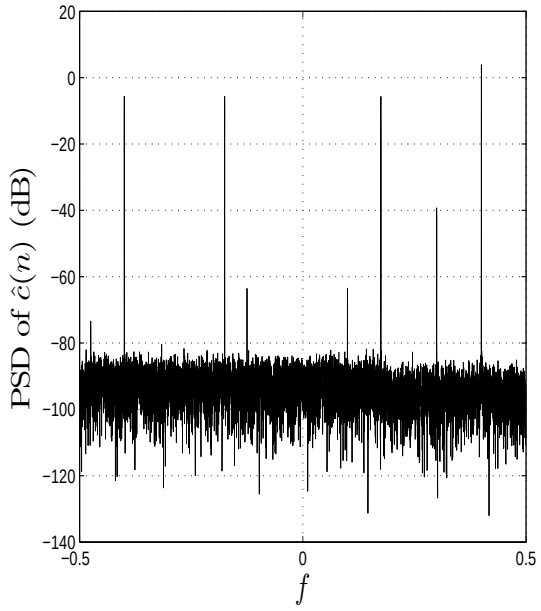

Fig. 9. PSD of the estimated envelope $\hat{c}(n)$ after calibration.

simulations for values of the carrier frequency F_c equal to 2.15, 3.15, 4.15 and 5.15GHz. The complex envelope signal $c_c(t)$ is given by (31) in all cases, and the sub-ADC sampling frequency $F_s' = 1$GHz, so that the values of the carrier frequency correspond to $\ell = 2$, 3, 4 and 5, and $\omega_b = 0.3\pi$ in all cases. For these signals, we select a nominal timing offset value equal to $d_0 = 1/2 - 3/(8\ell)$, which ensures d_0 does not correspond to a forbidden value. The gain and timing mismatches are still $\gamma = 10^{-2}$ and $\delta = -0.25 \times 10^{-2}$. For these simulation parameters, the MSE of the complex envelope error before and after calibration and the final estimates $\hat{\gamma}(L)$ and $\hat{\delta}(L)$ are shown in Table I. The table indicates that the performance of the complex envelope sampling scheme degrades steadily both before and after calibration as ℓ increases, and the MSE calibration improvement declines slightly from 25dB for $\ell = 2$ to 18dB for $\ell = 5$. The gain underestimate increases, but the accuracy of the the timing delay estimate does not suffer significantly when ℓ increases. Since other simulations not shown here indicate that gain mismatches have little effect on the envelope MSE, we conclude that the main reason for the loss of performance of the proposed calibration algorithm as ℓ increases is not the blind estimation algorithm, which estimates timing mismatches accurately, but the first-order approximation (13) and (14) of the reconstruction filters, which becomes progressively less accurate as ℓ increases. Thus for large ℓ, it may be desirable to include second-order terms in expansions (13) and (14). The presence of large higher-order terms is also the cause of the underestimation of the gain mismatch γ, since the analysis presented in [9, Sec. 4] for gain estimation of baseband sampling TIADCs shows that the presence of noise contributes to a negative bias in the gain estimate. For the case considered here, the higher order terms neglected in expansions (13) and (14) play the role of noise, which causes the gain mismatch underestimation.

Carrier Freq.	2.15GHz	3.15Gz	4.15GHz	5.15 GHz
MSE, Before (dB)	-25.51	-22.24	-19.76	-17.79
MSE, After (dB)	-50.89	-46.01	-40.97	-36.52
$\hat{\gamma}(L)(\times 10^{-3})$	10	9.7	8.8	7.7
$\hat{\delta}(L)$ $(\times 10^{-3})$	2.5	2.6	2.6	2.7

TABLE I. VARIATION OF THE MSE BEFORE AND AFTER CALIBRATION AND OF THE MISMATCH PARAMETER ACCURACY AS THE IMAGE ZONE INDEX ℓ INCREASES.

B. Bandlimited White Noise Compex Envelope

To demonstrate that the proposed blind estimation algorithm works satisfactorily for different types of complex envelope signals, for the case of a carrier frequency $F_c = 5.15$GHz, we consider the case where the complex envelope $c_c(t)$ is a bandlimited white noise signal with bandwidth $B/(4\pi) = 400$MHz. The sub-ADC sampling frequency remains $F_s' = 1$GHz, so that the oversampling ratio is again $\alpha = 0.2$. The PSD of the true sampled complex envelope is shown in Fig. 10. The nominal TIADC parameters $d_0 = 0.425$ and $g_0 = 1$, and mismatches γ and δ are the same as before. Since $\omega_b = 0.3\pi$ and $\ell = 5$, the reconstruction filters $H_{ij}(e^{j\omega})$, $i = 1, 2$ and $j = 0, 1$ and bandpass filter $H_{\rm BP}(e^{j\omega})$ are the same as in the earlier example.

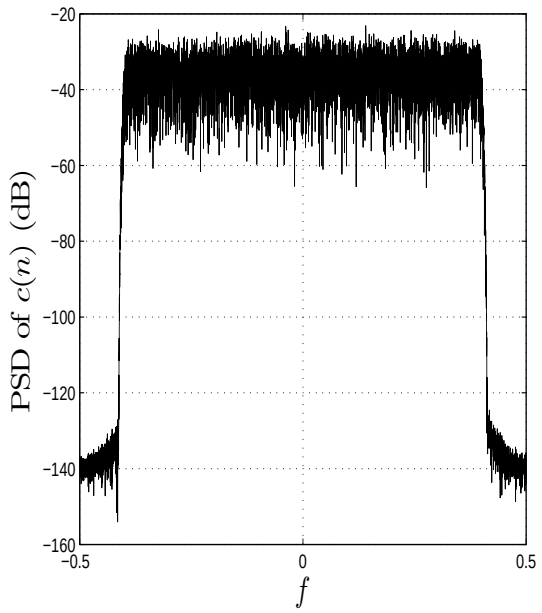

Fig. 10. PSD of the actual sampled bandlimited white noise complex envelope.

The blind estimation algorithm is applied to a data block of length $L = 10^5$ samples with adaptation step sizes $\mu_\gamma = 5 \times 10^{-4}$ and $\mu_\delta = 5 \times 10^{-6}$ and zero initial mismatch values. The resulting estimated mismatches are shown as a function

of time in Fig. 11 and Fig. 12. The final estimated gain and timing offset mismatches estimates are $\hat{\gamma}(L) = 0.83 \times 10^{-4}$ and $\hat{\delta}(L) = -0.24 \times 10^{-4}$. As in the case of a sum of complex tones envelope, the gain mismatch is understimated, but slightly less so than in the complex tone case, and the timing offset mismatch is estimated accurately. The MSE of the complex envelope error is -37.56dB.

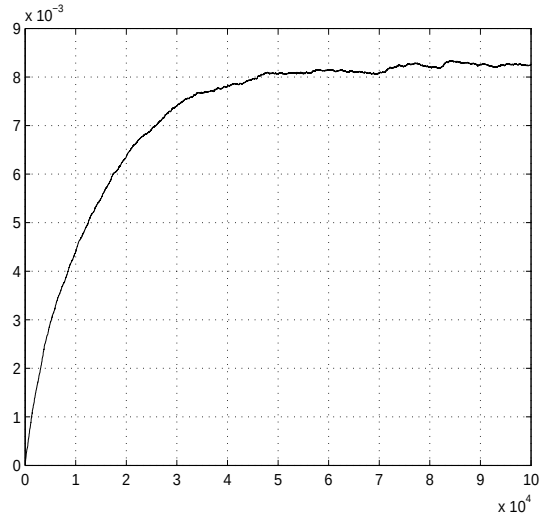

Fig. 11. Gain mismatch estimates for a bandlimited white noise complex envelope, with $L = 10^5$ samples, and adaptation step sizes $\mu_\gamma = 5 \times 10^{-4}$ amd $\mu_\delta = 5 \times 10^{-6}$.

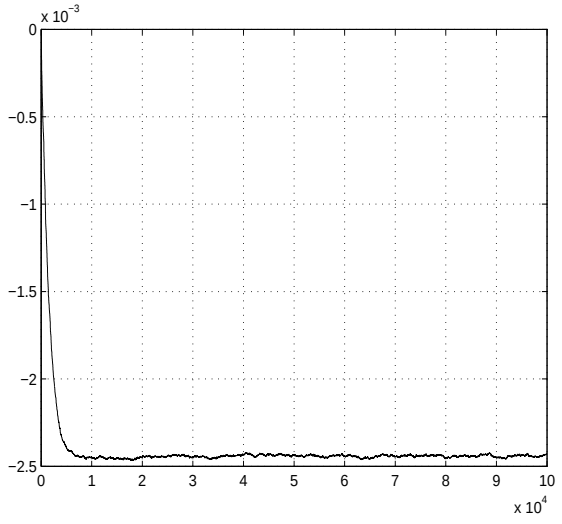

Fig. 12. Timing offset mismatch estimates for a bandlimited white noise complex envelope, with $L = 10^5$ samples, and adaptation step sizes $\mu_\gamma = 5 \times 10^{-4}$ amd $\mu_\delta = 5 \times 10^{-6}$.

Finally, the PSD of the complex envelope after calibration is shown in Fig. 13. The PSD is computed by selecting the final block of length $N = 10^4$ samples of the blind calibration simulation, after the estimation algorithm has converged.

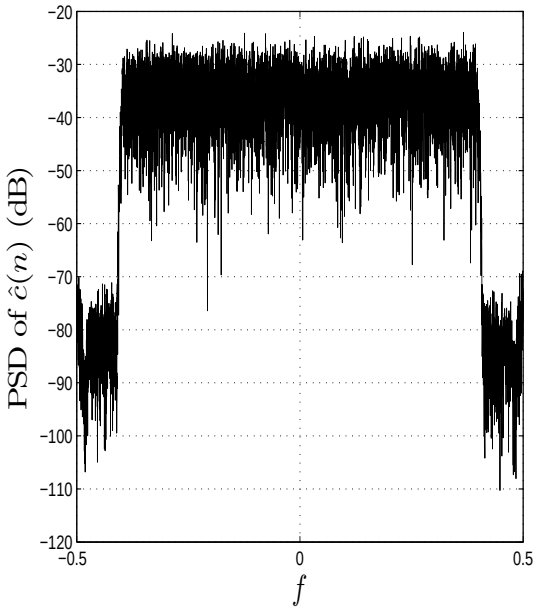

Fig. 13. PSD of the sampled bandlimited white noise complex envelope after calibration.

V. Conclusions

A blind calibration method has been proposed for calibrating a nonuniformly interleaved ADC used for sampling directly the complex envelope of a bandpass signal. The blind calibration method requires that the bandpass signal should be slightly oversampled, which ensures the presence of a frequency band over which the sampled complex envelope $c(n)$ has no power. By extracting the component of the reconstructed envelope corresponding to this frequency band, an error signal is obtained. This error signal can be minimized adaptively by using a stochastic gradient approach in order to obtain estimates of the TIADC gain and timing offset mismatches.

The adaptive complex envelope reconstruction structure used in Fig. 4 relies on *fixed* FIR filters and includes only three adaptive taps (two equal to $\hat{\delta}(n)$ and one equal to $\hat{\gamma}(n)$). Numerical simulations for a complex envelope formed by sums of complex tones, and for a bandlimited white noise complex envelope show that the calibration scheme can be effective for low or moderate values of the image index ℓ. For large values values of ℓ, i.e. for large carrier frequencies, higher order terms may be needed in the Taylor series approximations (13) and (14) of the reconstruction filters, which would increase significantly the complexity of the proposed calibration method. Alternatively, one may consider estimating adaptively the entire FIR impulse responses of filters H_1 and and H_2 to minimize error $e(n)$. This approach has a high computational complexity, but it could potentially correct additional sub-ADC impairments, such as bandwidth mismatches [10], [15]–[17].

APPENDIX A
IMPULSE RESPONSES OF THE GRADIENT FILTERS

The impulse responses of gradient filters $H_{11}(e^{j\omega})$ and $H_{22}(e^{j\omega})$ are obtained by taking the partial derivatives with respect to d of the impulse responses of the correction filters $h_1(n,d)$ and $h_2(n,d)$ given by (10) and (11). This gives

$$\Re\{h_{11}(n,d)\} = \Re\{h_{21}(n,d)\} = 0\,,$$

$$\begin{aligned}\Im\{h_{11}(n,d)\} &= \pi(2\ell+\mathrm{sgn}(\omega_b))\csc^2(\pi(2\ell+\mathrm{sgn}(\omega_b))d)\delta(n)\\ &\quad+\pi[2\ell\csc^2(2\pi\ell d)-(2\ell+\mathrm{sgn}(\omega_b))\csc^2(\pi(2\ell+\mathrm{sgn}(\omega_b))d)]\\ &\quad\times\frac{\sin((\pi-|\omega_b|)n)}{\pi n}\,,\end{aligned} \tag{34}$$

and

$$\begin{aligned}\Im\{h_{21}(n,\boldsymbol{\theta})\} &= \frac{1}{g\pi(n+d)}\\ &\quad\times\Big[(\pi-|\omega_b|)\frac{\cos((\pi-|\omega_b|)(n+d))}{\sin(2\pi\ell d)}\\ &\quad-2\pi\ell\frac{\sin((\pi-|\omega_b|)(n+d))\cos(2\pi\ell d)}{\sin^2(2\pi\ell d)}\\ &\quad+|\omega_b|\frac{\cos((\pi-|\omega_b|)(n+d)-\pi d)}{\sin(\pi(2\ell+\mathrm{sgn}(\omega_b))d)}\\ &\quad+\pi(2\ell+\mathrm{sgn}(\omega_b))\sin((\pi-|\omega_b|)(n+d)-\pi d)\\ &\qquad\times\frac{\cos(\pi(2\ell+\mathrm{sgn}(\omega_b))d)}{\sin^2(\pi(2\ell+\mathrm{sgn}(\omega_b))d)}\Big]\\ &\quad-\frac{1}{n+d}\Im\{h_2(n,\boldsymbol{\theta})\}\,.\end{aligned} \tag{35}$$

APPENDIX B
QUADRATIC APPROXIMATION OF $J(\hat{\boldsymbol{\theta}})$

To derive a quadratic approximation of $J(\hat{\boldsymbol{\theta}})$, we start by noting that the model of Fig. 2 implies that the DTFTs $X_1(e^{j\omega})$ and $X_2(e^{j\omega})$ of the sub-ADC sequences can be expressed in term of the DTFT $C(e^{j\omega})$ of complex envelope $c(n)$ as

$$\left[\begin{array}{c} X_1(e^{j\omega}) \\ F^{-1}(e^{j\omega})X_2(e^{j\omega}) \end{array}\right] = \mathbf{M}(e^{j\omega},d)\left[\begin{array}{c} C(e^{j(\omega-\omega_b)}) \\ C^*(e^{j(\omega+\omega_b)}) \end{array}\right] \tag{36}$$

where

$$\mathbf{M}(e^{j\omega},d) = \frac{1}{2}\left[\begin{array}{cc} 1 & 1 \\ G(e^{j\omega}) & G^*(e^{-j\omega}) \end{array}\right]. \tag{37}$$

Accordingly, the DTFT of signal $r(n,\hat{\boldsymbol{\theta}})$ in Fig. 4 can be expressed as

$$\begin{aligned} R(e^{j\omega},\hat{\boldsymbol{\theta}}) &= \left[\begin{array}{cc} H_1(e^{j\omega},\hat{d}) & H_2(e^{j\omega},\hat{\boldsymbol{\theta}}) \end{array}\right]\left[\begin{array}{c} X_1(e^{j\omega}) \\ X_2(e^{j\omega}) \end{array}\right]\\ &= \mathbf{L}(e^{j\omega},\hat{\boldsymbol{\theta}})\left[\begin{array}{c} C(e^{j(\omega-\omega_b)}) \\ C^*(e^{j(\omega+\omega_b)}) \end{array}\right] \end{aligned} \tag{38}$$

with

$$\begin{aligned}\mathbf{L}(e^{j\omega},\hat{\boldsymbol{\theta}}) &= [\,1\quad 0\,]\,\mathbf{M}^{-1}(e^{j\omega},\hat{d})\\ &\quad\times\left[\begin{array}{cc} 1 & 0 \\ 0 & \frac{g}{\hat{g}}e^{j\omega(\hat{d}-d)} \end{array}\right]\mathbf{M}(e^{j\omega},d)\,.\end{aligned} \tag{39}$$

By performing a first-order Taylor series expansion of $\mathbf{L}(e^{j\omega},\hat{\boldsymbol{\theta}})$ in the vicinity of $\boldsymbol{\theta}$, we find

$$\begin{aligned}\mathbf{L}(e^{j\omega},\hat{\boldsymbol{\theta}}) &\approx [\,1\quad 0\,]\\ &\quad+\epsilon\mathbf{L}_\gamma(e^{j\omega})+\eta\mathbf{L}_\delta(e^{j\omega})\,,\end{aligned} \tag{40}$$

with

$$\epsilon = \hat{\gamma}-\gamma\quad,\quad \eta = \hat{\delta}-\delta\,,$$

where

$$\begin{aligned}\mathbf{L}_\gamma(e^{j\omega}) &= -[\,1\quad 0\,]\,\mathbf{M}^{-1}(e^{j\omega},d)\\ &\quad\times\left[\begin{array}{cc} 0 & 0 \\ 0 & 1 \end{array}\right]\mathbf{M}(e^{j\omega},d)\end{aligned} \tag{41}$$

and

$$\begin{aligned}\mathbf{L}_\delta(e^{j\omega}) &= [\,1\quad 0\,]\,\mathbf{M}^{-1}(e^{j\omega},d)\\ &\quad\times\Big[j\omega\left[\begin{array}{cc} 0 & 0 \\ 0 & 1 \end{array}\right]\mathbf{M}(e^{j\omega},d)-\frac{\partial}{\partial d}\mathbf{M}(e^{j\omega},d)\Big]\,.\end{aligned} \tag{42}$$

We find

$$\frac{\partial}{\partial d}M(e^{j\omega},d) = \frac{1}{2}\left[\begin{array}{cc} 0 & 0 \\ J(e^{j\omega})G(e^{j\omega}) & J^*(e^{-j\omega})G^*(e^{-j\omega}) \end{array}\right] \tag{43}$$

where

$$J(e^{j\omega}) \triangleq \frac{\partial}{\partial d}\ln G(e^{j\omega})$$

is given by

$$J(e^{j\omega}) = \left\{\begin{array}{ll} -j2\pi(\ell+1) & -\pi\le\omega<-\pi+\omega_b \\ -j2\pi\ell & -\pi+\omega_b\le\omega<\pi\,, \end{array}\right.$$

for $\omega_b > 0$ and

$$J(e^{j\omega}) = \left\{\begin{array}{ll} -j2\pi\ell & -\pi\le\omega\le\pi+\omega_b \\ -j2\pi(\ell-1) & \pi+\omega_b\le\omega<\pi\,. \end{array}\right.$$

for $\omega_b < 0$. Then by observing that the bandpass filter $H_{\mathrm{BP}}(e^{j\omega})$ has been selected such that

$$H_{\mathrm{BP}}(e^{j\omega})C(e^{j(\omega-\omega_b)}) = 0\,, \tag{44}$$

we conclude that the DTFT of error signal $E(e^{j\omega},\hat{\boldsymbol{\theta}})$ can be expressed as

$$\begin{aligned}E(e^{j\omega},\hat{\boldsymbol{\theta}}) &= H_{\mathrm{BP}}(e^{j\omega})R(e^{j\omega},\hat{\boldsymbol{\theta}})\\ &\approx[\epsilon N_\gamma(e^{j\omega})+\eta N_\delta(e^{j\omega})]C^*(e^{-j(\omega+\omega_b)})\,,\end{aligned} \tag{45}$$

where after some substitutions, we find

$$\begin{aligned}N_\gamma(e^{j\omega}) &= H_{\mathrm{BP}}(e^{j\omega})L_\gamma(e^{j\omega})\left[\begin{array}{c} 0 \\ 1 \end{array}\right]\\ &= -H_{\mathrm{BP}}(e^{j\omega})[\,1\quad 0\,]\\ &\quad\times\mathbf{M}^{-1}(e^{j\omega},d)\left[\begin{array}{c} 0 \\ G^*(e^{-j\omega})/2 \end{array}\right]\\ &= \frac{1}{2}H_{\mathrm{BP}}(e^{j\omega})H_1(e^{j\omega},d)\,,\end{aligned} \tag{46}$$

and

$$\begin{aligned} N_\delta(e^{j\omega}) &= H_{\rm BP}(e^{j\omega})L_\delta(e^{j\omega}) \left[\begin{array}{c} 0 \\ 1 \end{array} \right] \\ &= (j\omega - J^*(e^{-j\omega}))H_{\rm BP}(e^{j\omega}) \left[\begin{array}{cc} 1 & 0 \end{array} \right] \\ &\quad \times \mathbf{M}^{-1}(e^{j\omega},d) \left[\begin{array}{c} 0 \\ G^*(e^{-j\omega})/2 \end{array} \right] \\ &= \frac{1}{2}(J^*(e^{-j\omega}) - j\omega)H_{\rm BP}(e^{j\omega})H_1(e^{j\omega},d)\,. \end{aligned} \quad (47)$$

in expression (45), $C^*(e^{-j(\omega+\omega_b)})$ represents the Fourier transform of signal

$$q(n) = e^{-j\omega_b n}c^*(n)\,.$$

To evaluate the power of $e(n,\hat{\boldsymbol{\theta}})$, we assume that the complex envelope process $c(n)$ is zero-mean WSS, i.e. that the complex autocorrelation function

$$R_c(m) = E[c(n+m)c^*(n)]$$

depends on m only. The power spectral density (PSD) of $c(n)$ is then defined as

$$S_c(e^{j\omega}) = \sum_{m=-\infty}^{\infty} R_c(m)e^{-jm\omega} \quad (48)$$

It is 2π-periodic and since autocorrelation $R_c(m)$ satisfies $R_c(m) = R_c^*(-m)$, it is real and non-negative (but not necessarily even). Then the autocorrelation of signal $q(n)$ is

$$R_q(n) = e^{-j\omega_b m}R_c(-m)$$

and its PSD is

$$R_q(e^{j\omega}) = S_c(e^{-j(\omega+\omega_b)})\,.$$

Expression (45) for the DTFT of error signal $e(n,\hat{\boldsymbol{\theta}})$ implies that it is also WSS with PSD

$$S_e(n,\hat{\boldsymbol{\theta}}) = \Big[\epsilon^2|N_\gamma(e^{j\omega})|^2 + \eta^2|N_\delta(e^{j\omega})|^2\Big]S_q(e^{j\omega})\,, \quad (49)$$

where the absence of cross-term is due to the fact that the real part of purely imaginary term $J^*(e^{-j\omega}) - j\omega$ is zero. By using this expression inside (18), we find that

$$\begin{aligned} J(\hat{\boldsymbol{\theta}}) &= \frac{1}{4\pi}\int_{-\pi}^{\pi} S_e(e^{j\omega},\hat{\boldsymbol{\theta}})d\omega \\ &= J_\gamma\epsilon^2 + J_\delta\eta^2 \end{aligned} \quad (50)$$

with

$$\begin{aligned} J_\gamma &= \frac{1}{4\pi}\int_{-\pi}^{\pi} |N_\gamma(e^{j\omega})|^2 S_q(e^{j\omega})d\omega \\ &= \frac{1}{16\pi}\int_{I_m} |H_1(e^{j\omega},d)|^2 S_c(e^{-j(\omega+\omega_b)})d\omega \end{aligned} \quad (51)$$

and

$$\begin{aligned} J_\delta &= \frac{1}{4\pi}\int_{-\pi}^{\pi} |N_\delta(e^{j\omega})|^2 S_q(e^{j\omega})d\omega \\ &= \frac{1}{16\pi}\int_{I_m} |J^*(e^{-j\omega}) - j\omega|^2|H_1(e^{j\omega},d)|^2 \\ &\qquad \times S_c(e^{-j(\omega+\omega_b)})d\omega\,. \end{aligned} \quad (52)$$

In equations (51) and (52), $I_m = I \mod (2\pi)$ is defined so that I_m is a subset of $[-\pi,\pi]$. Since $H_1(e^{j\omega},d)$ is a piecewise constant and nonzero filter, the expressions (51) and (52) imply that the coefficients J_γ and J_δ are nonzero, so that $J(\hat{\boldsymbol{\theta}})$ is a positive definite quadratic function of ϵ and η in the vicinity of $\boldsymbol{\theta}$, as long as signal $q(n) = e^{j\omega_b n}c^*(n)$ has some power in band I_m. Equivalently, $c(n)$ must have some power in the band

$$I_T = [(1-\alpha)\pi,(1+\alpha)\pi] - 2\omega_b \mod (2\pi)\,. \quad (53)$$

In this case $J(\hat{\boldsymbol{\theta}})$ will be minimized when $\epsilon = \eta = 0$, or equivalently when estimates $\hat{\gamma} = \gamma$ and $\hat{\delta} = \delta$ correspond to the true mismatch values.

At this point, it is worth noting that the band I_T has width $2\alpha\pi$ and is completely contained inside the spectral support region $[-(1-\alpha)\pi,(1-\alpha)\pi]$ of $c(n)$ as long as $\alpha\pi \le |\omega_b| \le (1-\alpha)\pi$. On the other hand when ω_b is located either close to the center of interval $[-\pi,\pi]$ (with $|\omega_b| < \alpha\pi$) or located close to its edges (with $|\omega_b \pm \pi| < \alpha\pi$, only part of I_T is located within the spectral support region $[-(1-\alpha)\pi,(1-\alpha)\pi]$ of $c(n)$. When ω_b is exactly equal to zero or $\pm\pi$, then I_T and the spectral support region $[-(1-\alpha)\pi,(1-\alpha)\pi]$ are disjoint, so that the calibration technique proposed here will not work as described. To deal with such cases, it would be useful to identify a frequency band other than I where $r(n,\boldsymbol{\theta}) = e^{-j\omega_b n}c(n)$ is free of energy, and then in the block diagram of Fig. 4, change the passband of filter $H_{\rm BP}$ to this zero energy band, so that condition (44) still holds.

At this point it is worth indicating that although it has been assumed that $c(n)$ is WSS in order to derive the closed-form expressions (52) and (53) for the coefficients J_γ and J_δ of the quadratic approximation (51) of $J(\hat{\boldsymbol{\theta}})$, this assumption was needed only for analysis purposes. The conclusion that $J(\hat{\boldsymbol{\theta}})$ is locally positive definite quadratic in the vicinity of $\boldsymbol{\theta}$ holds in general, even if $c(n)$ is nonstationary, as long as $c(n)$ has significant power in the frequency band I_T during segments of time which are long enough to ensure that the estimation algorithm (22) converges.

REFERENCES

[1] B. C. Levy, M. S. Wahab, and A. Van Selow, "Direct complex envelope sampling with nonuniformly interleaved two-channel ADCs." Submitted to IEEE TCAS II.

[2] A. Kohlenberg, "Exact interpolation of band-limited functions," *J. Applied Physics*, vol. 24, pp. 1432–1436, Dec. 1953.

[3] R. G. Vaughan, N. L. Scott, and D. R. White, "The theory of bandpass sampling," *IEEE Trans. Sig. Proc.*, vol. 39, pp. 1973–1984, Sept. 1991.

[4] J. G. Proakis and D. G. Manolakis, *Digital Signal Processing: Principles, Algorithms, and Applications, 4th edition*. Upper Saddle River, NJ: Prentice-Hall, 2007.

[5] A. J. Coulson, "A generalization of nonuniform bandpass sampling," *IEEE Trans. Sig. Proc.*, vol. 41, pp. 694–704, Mar. 1995.

[6] Y.-P. Lin and P. P. Vaidyanathan, "Periodically nonuniform sampling of bandpass signals," *IEEE Trans. Sig. Proc.*, vol. 45, pp. 340–351, Mar. 1998.

[7] W. Namgoong, "Finite-length synthesis filters for non-uniformly time-interleaved analog-to-digital converter," in *Proc. 2002 IEEE Internat. Conf. Circuits and Systems*, vol. 4, (Scottsdale, AZ), pp. 815–818, May 2002.

[8] F. Xu, "Perfect data reconstruction algorithm of time interleaved ADC," in *Proc. 2006 IEEE Internat. Test Conference*, (Santa Clara, CA), pp. 1–6, 2006.

[9] S. Huang and B. C. Levy, "Adaptive blind calibration of timing offset and gain mismatch for two-channel time-interleaved A/D converters," *IEEE Trans. Circuits Syst. I*, vol. 53, pp. 1278–1288, June 2006.

[10] S. Saleem and C. Vogel, "Adaptive blind background calibration of polynomial-represented frequency response mismatches in a two-channel time-interleaved ADC," *IEEE Trans. Circuits Syst. I*, vol. 58, pp. 1300–1310, June 2011.

[11] M. Seo, M. J. W. Rodwell, and U. Madhow, "Generalized blind mismatch correction for two-channel time-interleaved A-to-D converters," in *Proc. 2007 IEEE Conf. on Acoustics, Speech, and Signal Processing*, vol. 3, (Honolulu, HI), pp. 1505–1508, Apr. 2007.

[12] S. M. Jamal, D. Fu, M. P. Singh, P. J. Hurst, and S. H. Lewis, "Calibration of sample-time error in a two-channel time-interleaved analog-to-digital converter," *IEEE Trans. Circuits Syst. I*, vol. 51, pp. 130–139, Jan. 2004.

[13] J. Elbornsson, F. Gustafsson, and J.-E. Eklund, "Blind equalization of time errors in a time interleaved ADC system," *IEEE Trans. Sig. Proc.*, vol. 53, pp. 1413–1424, Apr. 2005.

[14] J. Matsuno, T. Yamaji, M. Furuta, and T. Itakura, "A fully digital background calibration technique for time-interleaved ADC using pseudo aliasing signal," *IEEE Trans. Circuits Syst. I*, vol. 60, pp. 1113–1121, May 2013.

[15] T.-H. Tsai, P. J. Hurst, and S. H. Lewis, "Bandwidth mismatch and its correction in time-interleaved analog-to-digital converters," *IEEE Trans. Circuits Syst. II*, vol. 53, pp. 1133–1137, Oct. 2006.

[16] H. Johansson, "A polynomial-based time varying filter structure for the compensation of frequency-response mismatch errors in time-interleaved ADCs," *Selec. Topics in Signal Proc.*, vol. 3, pp. 384–396, 2009.

[17] P. Satarzadeh, B. C. Levy, and P. J. Hurst, "Adaptive semiblind calibration of bandwidth mismatch for two-channel time-interleaved ADCs," *IEEE Trans. Circuits Syst. I*, vol. 56, pp. 2075–2088, Sept. 2009.

[18] F. Harris, X. Chen, E. Venosa, and F. A. N. Palmieri, "Two-channel TI-ADC for communication signals," in *Proc. 2001 IEEE 12th Internat. Workshop on Signal Proc. Advances in Wireless communications (SPAWC' 11)*, (San Francisco, CA), pp. 576–580, June 2011.

[19] F. J. Harris, "Artifact-corrected time-interleaved ADC." US Patent No. 8,957,798, Feb. 2015.

[20] M. Waltari, "Time-interleaved analog-to-digital converter for signals in any Nyquist zone." US Patent No. 8,654,000, Feb. 2014.

[21] H. L. Duc, C. Jabbour, P. Desgreys, O. Jamin, and V. T. Nguyen, "A fully digital background calibration of timing skew in undersampling TI-ADC," in *Proc. 12th IEEE Internat. New Circuits and Systems Conf. (NEWCAS'14)*, (Trois Rivières, Canada), pp. 53–56, June 2014.

[22] H. Robbins and S. Monro, "A stochastic approximation method," *Annals Math. Stat.*, vol. 22, pp. 400–407, 1951.

[23] L. Ljung and T. Soderstrom, *Theory and Practice of Recursive Identification*. Cambridge, MA: MIT Press, 1983.

[24] A. Benveniste, M. Métivier, and P. Priouret, *Adaptive Algorithms and Stochastic Approximations*. Berlin: Springer Verlag, 1990.

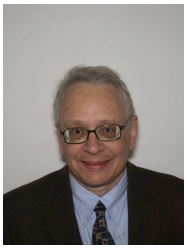

Bernard C. Levy received the diploma of Ingénieur Civil des Mines from the Ecole Nationale Supérieure des Mines in Paris, France in 1974, and the Ph.D. in Electrical Engineering from Stanford University in 1979.

From July 1979 to June 1987 he was Assistant and then Associate Professor in the Department of Electrical Engineering and Computer Science at M.I.T. Since July 1987, he has been with the University of California at Davis, where he is Professor of Electrical Engineering and a member of the Graduate Group in Applied Mathematics. He served as Chair of the Department of Electrical and Computer Engineering at UC Davis from 1996 to 2000. He was a Visiting Scientist at the Institut de Recherche en Informatique et Systèmes Aléatoires (IRISA) in Rennes, France from January to July 1993, and at the Institut National de Recherche en Informatique et Automatique (INRIA), in Rocquencourt, France, from September to December 2001. He is the author of the book *Principles of Signal Detection and Parameter Estimation* (New York, NY: Springer, 2008). His research interests include statistical signal processing, estimation, detection, and circuits applications of signal processing.

Dr. Levy served as Associate Editor of the IEEE Transactions on Circuits and Systems I, of the IEEE Transactions on Circuits and Systems II, and of the EURASIP J. on Advances in Signal Processing. He is currently an Associate Editor of Signal Processing. He is a member of SIAM.

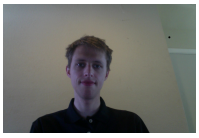

Anthony Van Selow received his BS in Electrical Engineering from UC Davis in 2012 and is currently completing a MS in Electrical Engineering at UC Davis. He worked as an intern at Dysonics from 2012 to 2014 and at Exponent from 2010 to 2011. His research interests include statistical signal processing, circuits applications of signal processing, and adaptive filtering.

Mansoor Wahab was born in Kabul, Afghanistan in January 1993 and immigrated to the United States in 2006. He completed his BS in Electrical Engineering with highest honors at UC Davis in June 2014. In his undergraduate studies he focused on signal processing and performed research on bandpass sampling and ADC calibration. He is currently a PHD student in the Electrical and Computer Engineering Department at Cornell University where his research has shifted towards optimal control theory and its applications to multiagent systems. Mr. Wahab's honors include an ECE Department Citation from UC Davis and a Cornell Dean's Excellence Fellowship for his first year of graduate studies. He is a student member of IEEE and plans to pursue an academic career.